Journal of Applied and Natural Science
17(1), 205 - 217 (2025)
ISSN : 0974-9411 (Print), 2231-5209 (Online)
journals.ansfoundation.org

Research Article

A new spectral index for vegetation extraction using satellite data

Arindom Ain*
Department of Computer Science and Engineering, Girijananda Chowdhury Institute of Management and Technology (GIMT), Under Assam Science and Technology University, Guwahati (Assam), India
Minakshi Gogoi
Department of Computer Science and Engineering, GCU Guwahati (Assam), India
Dibyajyoti Chutia
North Eastern Space Applications Centre (NESAC), Department of Space, Umium, Shillong (Meghalaya), India

*Corresponding author. E-mail: ainarindom@gmail.com

Article Info
https://doi.org/10.31018/jans.v17i1.6186
Received: September 14, 2024
Revised: February 14, 2025
Accepted: February 19, 2025

How to Cite
Ain, A. *et al.* (2025). A new spectral index for vegetation extraction using satellite data. *Journal of Applied and Natural Science*, 17(1), 205 - 217. https://doi.org/10.31018/jans.v17i1.6186

Abstract
Accurate vegetation extraction is essential for environmental monitoring, agricultural management, and ecosystem analysis applications. Traditional spectral indices, however, often suffer from reduced accuracy and sensitivity under varying environmental conditions. This research aimed to address these limitations by introducing a novel spectral index, "A New Vegetation Index" (ANVI), specifically designed for enhanced vegetation extraction for satellite imagery. ANVI leverages multiple spectral bands, including near-infrared (NIR), shortwave infrared (SWIR), and visible bands, commonly available in remote sensing data. The research involves implementing ANVI within a remote sensing framework and conducting a comparative analysis against established indices across diverse geographic regions. Key metrics such as accuracy, resilience to atmospheric disturbances, and sensitivity to soil background influences were evaluated. The results demonstrated that ANVI achieved a superior overall accuracy of 97.08% in vegetation classification and greater robustness against atmospheric noise than conventional indices. Furthermore, ANVI reduced soil background influence by significantly improving its performance under complex environmental conditions. This research highlights the novelty of ANVI as a computationally efficient and reliable tool for large-scale vegetation monitoring, offering enhanced precision and adaptability for diverse applications in remote sensing and ecological management

Keywords: Multispectral, Spectral Analysis, Spectral Incides, Vegetation Index

INTRODUCTION

Vegetation plays a vital role in Earth's ecosystems, significantly influencing climate regulation (Alkama *et al.,* 2022), hydrological cycles (Makarieva *et al.,* 2010), and various biological processes (Bendig *et al.,* 2015). It is a key indicator of global vegetation dynamics and climate change (Li *et al.,* 2020; Bendig *et al.,* 2015; Llobera, 2007). The accurate extraction of vegetation is essential for effective regional planning, sustainable development, and ecological conservation (Anderson *et al.,* 2016; Wang *et al.,* 2024; Hmimina *et al.,* 2013). Advancements in remote sensing technology, particularly through satellite platforms, have revolutionized vegetation monitoring (Mashala *et al.,* 2023). These technologies offer significant advantages over traditional methods. Spectral indices derived from remote sensing data have been extensively used in vegetation analysis, providing detailed insights into vegetation characteristics, crop growth, ecological quality, and surface conditions (Xue and Su, 2017; Clevers and Gitelson, 2013; Li *et al.,* 2017; Fu *et al.,* 2020; Delegido *et al.,* 2013). These advancements have significantly contributed to the field of vegetation monitoring and analysis (Hmimina *et al.,* 2013; Sun *et al.,* 2021). However, this process is challenging, especially in heterogeneous landscapes with a mix of landforms, including urban areas, agricultural fields, forests, and water bodies (Weng, 2012; Lu *et al.,* 2014). Spectral similarities among different land cover types in these regions often lead to confusion in image classification. Additionally, the classification of vegetation and non-vegetation depends on various factors, such as the spatial and spectral resolution of the images (Poursanidis *et al.,* 2015;

Ustuner and Sanli, 2015).

Vegetation indices are crucial in improving image classification accuracy by providing insights into moisture content, nutrient levels, and crop health (Clevers and Gitelson, 2013; Li *et al.,* 2017). Popular indices like the Normalized Difference Vegetation Index (NDVI) and the Enhanced Vegetation Index (EVI) are widely used for vegetation monitoring (Lane *et al.,* 2014; Au, 2023). EVI improves upon NDVI by correcting for atmospheric conditions and canopy noise, making it particularly useful in complex canopy. The Soil-Adjusted Vegetation Index (SAVI) further modifies NDVI by introducing a soil brightness correction factor, enhancing its accuracy in sparse vegetation (Ain *et al.,* 2021).

In this present research, the proposed index aimed to address the limitations of existing indices, particularly in diverse terrains where spectral overlaps and environmental conditions present significant challenges. The research focused on developing a new spectral index for extracting vegetation using Sentinel-2B imagery. It was designed to provide valuable tools for ecological monitoring and management.

MATERIALS AND METHODS

Test sites

The research identified three distinct test locations in Assam State (26.2006° N, 92.9376° E): Fig. 1(a) Test Site 1 (TS1), Fig. 1(b) Test Site 2 (TS2), and Fig. 1(c) Test Site 3 (TS3). Assam, spanning 78,438 sq. km, encompassed diverse landscapes, including densely built-up areas, various vegetation types (shrubs, forests, croplands, grasslands), water bodies, and open land. These sites were selected for their varied characteristics to evaluate the performance of the proposed indices across different landscapes. Vegetation features included all plant cover types, while non-vegetation features comprised built-up areas, water bodies, and open land. The test sites also included noise elements such as building shadows and cloud shadows to assess the robustness of the proposed vegetation index.

Image data

The imagery used in this research was sourced from Sentinel-2B, captured on June 17th, 2024, via the European Space Agency's Copernicus Open Access Hub. Sentinel-2B was selected for its superior spatial and spectral capabilities. Detailed information on its spectral bands is presented in Table 1. The images were georeferenced to WGS84 (EPSG:7758 for Assam), and atmospheric corrections and reflectance transformations were performed using the Semi-Automatic Classification Plugin (SCP) in QGIS (Tempa and Aryal, 2022; Congedo, 2021). The raw digital numbers (DNs) were converted to reflectance values following the method described by Markham and Barker (1986).

Six key spectral bands from Sentinel-2B were selected due to their relevance in vegetation studies: Bands 2 (Blue), 3 (Green), 4 (Red), 8 (Near-Infrared), 11, and 12 (Short-Wave Infrared). Bands 11 and 12, originally at a resolution of 20 meters, were resampled to 10 meters using bilinear resampling, which averages the four nearest pixels of the original raster (Singh and Bhide, 2016). This ensured a consistent resolution across all selected bands.

The significance of the spectral bands for vegetation analysis is summarized as follows:

Red (R): Assessed chlorophyll absorption and vegetation health, aiding in monitoring plant stress across varied environments.

Green (G): Indicated the green pigment in plants and distinguish between different vegetation types.

Blue (B): Though less frequently used alone, it en-

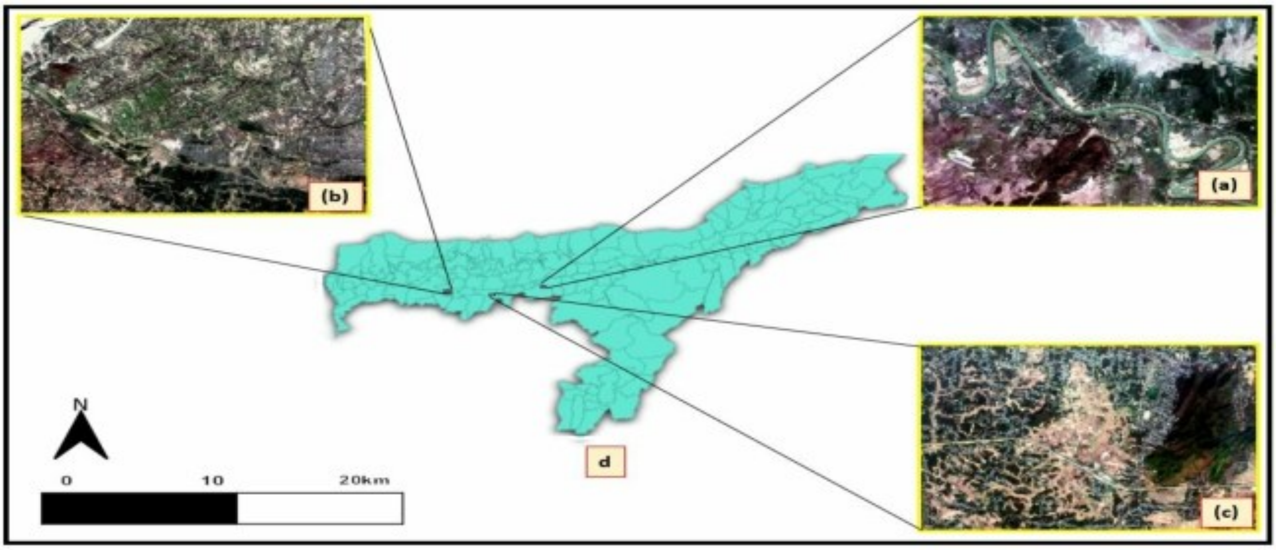

Fig 1. *(a) Test Site 1 (TS1) (b) Test Site 2 (TS2) (c) Test Site 3 (TS3) (d) Assam State*

Table 1. Sentinel 2B bands

Band Name	Central wavelength (nm)	Spatial resolution (m)
Band 1 Coastal aerosol	442.2	60
Band 2 – Blue	492.1	10
Band 3 – Green	559.0	10
Band 4 – Red	664.9	10
Band 5 – Vegetation red edge	703.8	20
Band 6 – Vegetation red edge	739.1	20
Band 7 – Vegetation red edge	779.7	20
Band 8 – NIR	832.9	10
Band 8A – Narrow NIR	864.0	20
Band 9 – Water vapour	943.2	60
Band 10 – SWIR – Cirrus	1376.9	60
Band 11 – SWIR	1610.4	20
Band 12 – SWIR	2185.7	20

hanced contrast in vegetative cover when combined with other bands.

Near-Infrared (NIR): Essential for vegetation monitoring, as healthy vegetation strongly reflects in this spectrum.

Short-Wave Infrared (SWIR): Detected soil and vegetation moisture, aiding in drought monitoring and plant stress assessment.

Multispectral data

The present research is grounded in multispectral satellite imagery, providing images captured across various electromagnetic spectrum wavelengths. Unlike traditional single-band images, multispectral data offered a detailed view of the Earth's surface by integrating information from multiple spectral bands (Ain *et al.,* 2021 and 2024). This data facilitated the creation of vegetation maps and supported monitoring changes over time. Precision agriculture also benefited from multispectral imagery by enabling the monitoring of crop health, optimizing irrigation, and improving yield prediction.

Spectral indices

Several spectral indices were employed to enhance vegetation monitoring and extraction from multispectral imagery. The NDVI, introduced by Rouse *et al.* (1974), was used to assess vegetation health by leveraging the reflectance differences between red and near-infrared bands, with values ranging from -1 to +1 (Gessesse

Table 2. Vegetation indices

Indices	Formulae	Threshold	Reference
NDVI	$(nir - red)/(nir + red)$	0.2-0.9	(USGS NDVI, 2024)
EVI	$\frac{2.5 * (nir - red)}{(nir + 6 * red - 7.5 * blue) + 1}$	0.2-0.8	(EOS EVI, 2024)
ARVI	$\frac{nir - 2 * red + blue}{nir + 2 * red + blue}$	0.2-0.8	(Sentinel Hub, 2024)
MSAVI	$\frac{2 * nir + 1 - \sqrt{(2 * nir + 1)^2 - 8 * (nir - red)}}{2}$	0.2-0.4	(EOS MSAVI, 2024)
SAVI	$\frac{1.5 * (nir - red)}{nir + red + 0.5}$	0.2-0.4	(USGS SAVI, 2024)
MGRVI	$\frac{green^2 - red^2}{green^2 + red^2}$	0.214	(Chen et al. 2024, Bendig et al. 2015)
IRGBVI	$(5 * green^2 - 2 * red^2 - 5 * blue^2)/(5 * green^2 + 2 * red^2 + 5 * blue^2)$	0.035-0.1	(Chen, 2024)
TBDVI	$\frac{nir - (red + swir1)}{2}$	0.07	(Zhao, 2024)

and Melesse, 2019). However, NDVI's sensitivity to atmospheric effects, soil brightness, and saturation in dense vegetation (Tucker, 1979) necessitated alternative indices. The Soil-Adjusted Vegetation Index (SAVI), proposed by Huete (1988), incorporated a soil correction factor (L) to minimize soil brightness effects, making it suitable for sparse vegetation. The Modified Soil-Adjusted Vegetation Index (MSAVI), developed by Qi *et al.* (1994), further refined this approach by dynamically adjusting the soil correction factor based on vegetation density. To address atmospheric disturbances, the Atmospherically Resistant Vegetation Index (ARVI) by Kaufman and Tanre (1992) introduced corrections for aerosol scattering, improving vegetation monitoring in polluted environments. The Enhanced Vegetation Index (EVI), developed by Huete et al. (2002), was employed for dense biomass. It incorporated coefficients to correct for atmospheric conditions and canopy background noise, making it effective for dense vegetation monitoring (Jiang *et al.,* 2008).

Other indices were used for specialized applications. The Green Normalized Difference Vegetation Index (GNDVI), introduced by Gitelson *et al.,* (1996), enhanced sensitivity to chlorophyll content, aiding crop health assessment. The Normalized Difference Water Index (NDWI) by Gao (1996) helped monitor vegetation moisture content and distinguish between vegetation and non-vegetation. The Renormalized Difference Vegetation Index (RDVI), proposed by Roujean and Breon (1995), combined NDVI and SAVI's strengths to improve sensitivity to vegetation density. The Normalized Burn Ratio (NBR), developed by Key et al.,(2006), was utilized for assessing fire-affected areas and post-fire vegetation recovery. Bendig *et al.,* (2015) developed the Modified Green–Red Vegetation Index (MGRVI) for biomass estimation during early growth stages. Chen *et al.* (2024) introduced the Improved-Red-Green-Blue Vegetation Index (IRGBVI) for plateau regions, achieving high accuracy in vegetation extraction by mitigating interference from features like blue roofs. Zhao *et al.* (2024) proposed the Three-Band Difference Vegetation Index (TBDVI) for detecting vegetation destruction events, outperforming indices like NDVI and NBR with better background interference reduction and cross-sensor applicability. Despite advancements, Xie *et al.,* (2008, 2022) and Buma *et al.* (2024) noted challenges in complex terrains, such as spectral overlaps and atmospheric interferences, highlighting the need for improved indices.

Thresholding

Thresholding methods play a crucial role in distinguishing vegetation from non-vegetation in multispectral satellite imagery. While techniques like Otsu's method (Xu, 2006; Zhai, 2015) enhance precision, they often add algorithmic complexity. Many indices, including those by McFeeters (1996), Rokni (2014), Rouse (1974), Feyisa (2014), Xu (2006), and Wilson (2002), adopt a zero-threshold approach for simplicity. Following this principle, the proposed index in this research also utilises a zero-threshold vegetation extraction method to ensure computational efficiency.

Reference data to verify the classification accuracy

Several studies recommended using high-resolution imagery with human intervention to obtain reference data (Feyisa *et al.,* 2014; Yan *et al.,* 2020). Vegetation was visually distinguished from non-vegetation using high-resolution Google Earth imagery (Au, 2023 and Ain, 2024). Vegetation boundaries were manually digitized from Google Earth imagery to generate reference data for test sites TS1, TS2, and TS3, ensuring alignment with their spatial extents. This reference data was utilized to evaluate the extraction accuracy of the vegetation indices. High-resolution images corresponding to the periods of the test sites were obtained and are shown in Fig. 2 (a) to (c). The distribution of pixels, total area, and number of polygons in the reference data are detailed in Table 3. These labeled maps exclusively served as ground truth for validating the classification results.

Accuracy assessment

The accuracy of the proposed index was evaluated by counting correctly and incorrectly classified vegetation pixels. Metrics such as overall accuracy (OA) and kappa coefficient (KC) were calculated using a confusion matrix (CM) (Khalid et al., 2021; Yan et al., 2020; Mondejar and Tongco, 2019), which compared predicted and actual class labels. The CM included the following components, as described in Table 4:

True Positives (TP): Instances where vegetation pixels were correctly classified as vegetation.

False Negatives (FN): Instances where vegetation pixels were incorrectly classified as non-vegetation.

False Positives (FP): Instances where non-vegetation pixels were incorrectly classified as vegetation.

True Negatives (TN): Instances where non-vegetation pixels were correctly classified as non-vegetation.

Additional metrics used in the accuracy assessment, including their definitions, are presented in Equations (1) through (5) in Table 5.

Proposed Index

This research followed a systematic, multi-step approach to ensure precise vegetation extraction and accurate analysis. The methodology comprised the following key stages:

Spectral Curve Generation: Development of spectral curves reflecting vegetation-specific characteristics.

Spectral Curve Analysis: Analysis of spectral reflec-

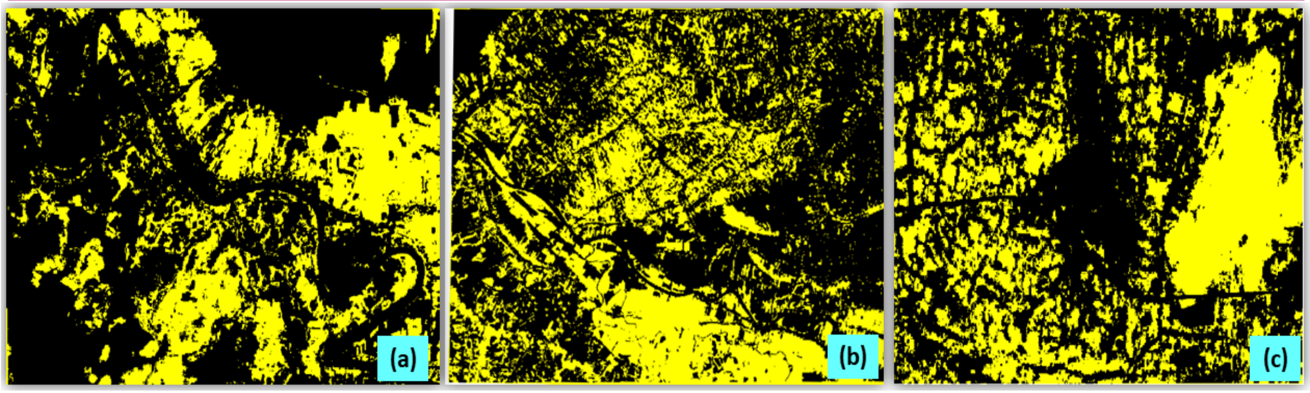

Fig 2. *Reference images of (a)TS1 (b)TS2 (c)TS3*

tance patterns for vegetation regions.

Formulation of Vegetation Index: Design of a novel index specific for vegetation extraction.

Optimization of the Proposed Index: Refinement of the formulated index to enhance its performance.

Complexity Analysis: Assessment of the computational efficiency of the proposed index.

Generating a spectral curve for vegetation regions

Spectral curve analysis was carried out to understand reflectance patterns and characterize vegetation features across diverse regions (Wang *et al.,* 2024; Shen *et al.,* 2008; Zagajewski
1*et al.,* 2017). Diverse vegetation types, including forests, grasslands, and croplands, were considered, as their spectral properties are influenced by factors such as soil type, moisture, and species composition (Yaseen and Wang*,* (2022); Roy 1989). Urban features and cloud shadows, which introduce additional complexity, were also analyzed. A systematic sampling strategy was employed, collecting over 50 sample points from randomly selected vegetation across various geographic locations. For each vegetation pixel, spectral reflectance values across multiple bands were recorded. The average reflectance values for vegetation across bands followed a consistent trend: $\rho_{nir} > \rho_{swir1} > \rho_{swir2} > \rho_{green} > \rho_{red} > \rho_{blue}$.

Spectral curve analysis of vegetation regions

The spectral curve analysis revealed critical insights into reflectance trends for vegetation pixels across multiple bands. Notably, the NIR band exhibited the highest reflectance due to strong reflection by the cellular structure of plant leaves (Jiang *et al.,* 2008), making it a definitive indicator of vegetation. Conversely, the BLUE band demonstrated minimal reflectance as chlorophyll absorbs blue light during photosynthesis (Papoutsis *et al.,* 2019). Reflectance increased in the GREEN band due to reduced chlorophyll absorption, producing vegetation's signature green hue. The RED band exhibited moderate reflectance, while the SWIR bands demonstrated decreasing trends, reflecting their sensitivity to leaf water content (Ceccato *et al.,* 2001). These distinct spectral characteristics were instrumental in accurately identifying and distinguishing vegetation from other land cover types.

Formulation of a new index for extraction of vegetation

The analysis of spectral curves revealed distinct variations among the values of six bands in vegetation, with noticeable normalized differences between them. This suggested that each band significantly contributed to the reflectance properties of vegetation pixels. Further observations highlighted unique trends in the NIR bands. Based on these insights, a new vegetation index was proposed, as shown in Equation (6):

$$ANVI = \rho_{nir} + \rho_{swir1} + \rho_{red} - \lambda * (\rho_{swir2} + \rho_{green} + \rho_{blue}) \quad (6)$$

Here, $\boldsymbol{\rho}$ represents the reflectance values of respective bands, and $\boldsymbol{\lambda}$ is an empirical parameter used to calibrate noise levels across test sites. The difference consistently resulted in positive values for vegetation pixels and negative values for non-vegetation pixels, ranging between -1 and +1.

Optimization of proposed expression for vegetation extraction

The proposed vegetation index was optimized through a recursive elimination approach, systematically excluding one or more spectral bands and evaluating performance. The blue band was found to significantly impact accuracy, and its exclusion led to notable performance drops. Similarly, the green band, though less impactful than blue, still influenced accuracy. The SWIR1 and SWIR2 bands were particularly essential in distinguishing vegetation in challenging conditions. Excluding multiple bands, such as blue and green or SWIR2 and blue, further degraded accuracy, emphasizing the interdependence of spectral bands. The NIR bands consistently played a pivotal role in maintaining accuracy across all scenarios. Detailed results of these

Table 3. Number of pixels, polygons and area

Items	TS1	TS2	TS3
Vegetation Pixels	94,421	264,701	98,148
Non-Vegetation Pixels	214,459	435,231	158,088
Polygon cover with vegetation pixels	1,400	4,297	1,761
Total Area (m2)	3,088,800	6,999,320	2,562,360

Table 4. *Confusion matrix for binary classification*

Items	Predicted Vegetation	Predicted Non-Vegetation
Actual Vegetation	TP	FN
Actual Non- Vegetation	FP	TN

evaluations for test sites TS1, TS2, and TS3 are presented in Table 6.

Complexity analysis

The complexity of the proposed vegetation index was analyzed in terms of time, space, and computational cost. The time complexity was determined to be O (M×N), where M represents the number of spectral bands and N the number of pixels, resulting in a linear computational time. Similarly, the space complexity was also O(M×N), accounting for memory requirements. The inclusion of the empirical parameter **λ** allowed fine-tuning of algorithm performance, influencing computational costs. This linear relationship ensured that the index remained efficient for varied datasets.

RESULTS AND DISCUSSION

Numerous vegetation indices have been developed to aid in satellite image classification, focusing on understanding vegetation health and monitoring related features. This section evaluates the effectiveness of the proposed vegetation index ANVI. The evaluation includes a comparative analysis against established vegetation indices from prior studies (Rouse et al., 1974; Kaufman and Tanre (1992); Qi et al., 1994; Huete, (1988); Huete et al., 2002, Bendig et al., 2015; Chen et al., 2024; Zhao et al., 2024). Binary classification maps for vegetation cover extraction generated for each test site (TS1-TS3) using all indices are listed in Table 1, depicted in Figures 4-6 respectively. A standardized set of metrics suitable for all test regions was utilized to quantitatively assess index performance. A detailed comparison of each index's classification performance with ANVI is presented in Tables 7 to 9. The analysis of vegetation indices from the data in TS1, TS2, and TS3 highlights the varying performances of these indices across different test sites, reflecting their distinct strengths and weaknesses in vegetation classification. The white rectangles in the indices images indicate pixels where some vegetation pixels are misclassified as non-vegetation pixels.

Additionally, it was observed that some vegetation covered in shadow are misclassified as non-vegetation. Furthermore, some non-vegetation pixels were classified as vegetation pixels, as indicated by the red circles in the indices images. NDVI consistently demonstrated the lowest performance across all test sites, with overall accuracy of 0.440 in TS1, 0.423 in TS2, and 0.430 in TS3. Despite marginal improvements in TS1, its Kappa coefficients remained below 0.12, indicating poor reliability. High Type I Errors (e.g., 0.789 in TS1) and Type II Errors (e.g., 0.128 in TS2) further underscore its inability to handle environmental variability effectively.

Table 5. Metrics used in the evaluation of vegetation indices

Evaluation Metrics	Description	Expression
Precision	The ratio of predictions as the positive class was positive.	$$\frac{TP}{TP+FP} \quad (1)$$
Recall	Measures what fraction of all positive samples were correctly predicted as positive by the classifier.	$$\frac{TP}{TP+FN} \quad (2)$$
F1-score	F1-score Harmonic mean of precision and recall.	$$2*\frac{precision*recall}{precision+recall} \quad (3)$$
Type I Error	Type I Error Instances are falsely classified as positive when they are negative.	$$\frac{FP}{TN+FP} \quad (4)$$
Type II Error	Type II Error Instances are falsely classified as negative when they are positive	$$\frac{FN}{TP+FN} \quad (5)$$

Table 6. Impact of band exclusion on vegetation extraction accuracy and kappa coefficient

Band Excluded	TS1		TS2		TS3	
	Overall Accuracy	**Kappa Coefficient**	**Overall Accuracy**	**Kappa Coefficient**	**Overall Accuracy**	**Kappa Coefficient**
Blue	0.4153	0.1028	0.4600	0.1028	0.4243	0.0520
Green	0.4054	0.0930	0.4344	0.0699	0.4136	0.0383
Red	0.7045	0.0457	0.6536	0.1024	0.6196	0.0086
SWIR1	0.7045	0.0457	0.6536	0.1024	0.6196	0.0086
SWIR2	0.4888	0.1796	0.5397	0.2098	0.3873	0.0053
Blue and Green	0.3057	0.0316	0.3783	0.0001	0.3832	0.0002
SWIR1 and Red	0.7045	0.0457	0.6536	0.1024	0.6196	0.0086
SWIR1 and SWIR2	0.8354	0.5495	0.9019	0.7909	0.7060	0.4189
SWIR2 and Blue	0.3486	0.0387	0.3913	0.0161	0.3835	0.0005
SWIR2 and Green	0.3452	0.0356	0.3897	0.0141	0.3833	0.0003
SWIR2 and Red	0.8032	0.4358	0.7402	0.3619	0.7532	0.4060

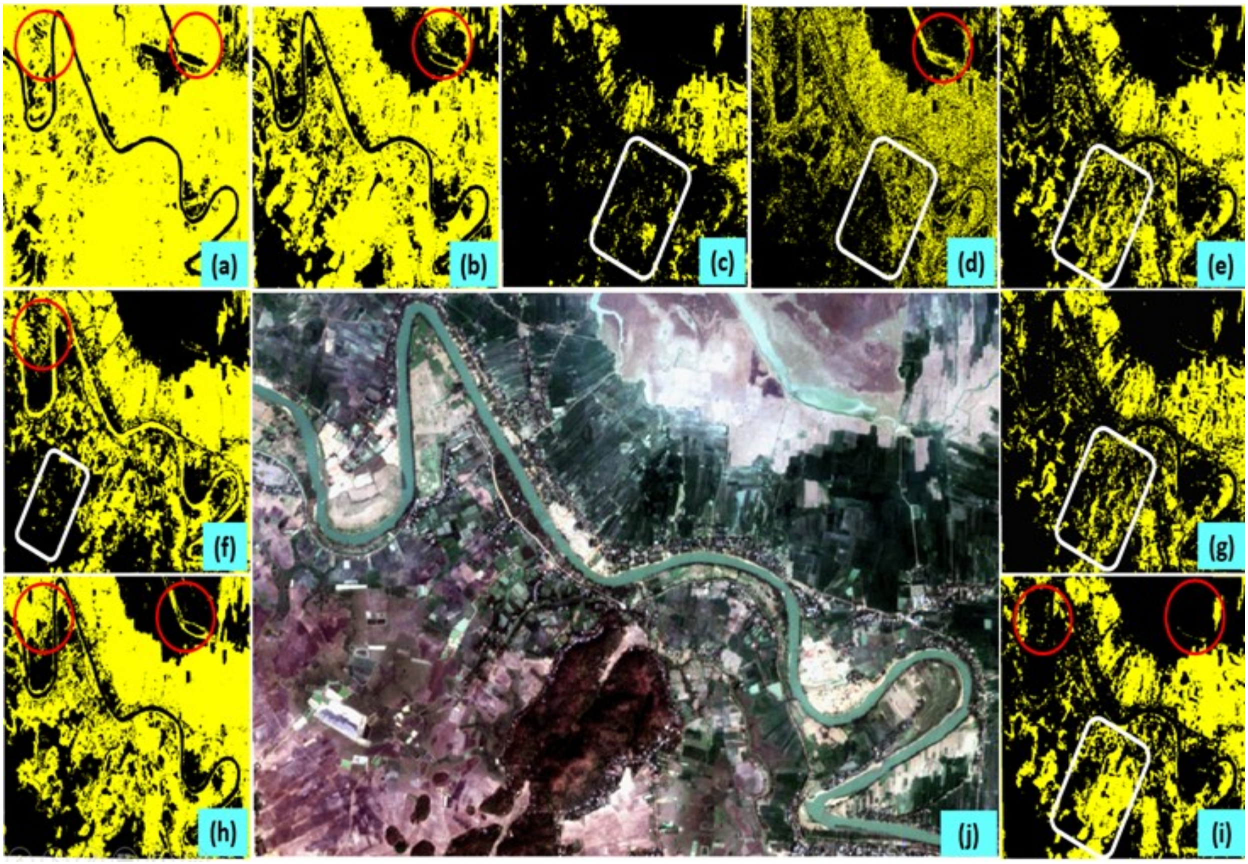

Fig 4. *Comparison of various vegetation indices with ANVI for TS1 (a) NDVI (b) ARVI (c) MSAVI (d) IRGBVI (e) EVI (f) MGRVI (g) SAVI (h) TBDVI (i) ANVI (j) RGB Image*

NDVI's reliance on only red and near-infrared bands makes it highly sensitive to atmospheric effects and soil brightness. ARVI addressed some limitations of NDVI by incorporating atmospheric resistance, achieving higher accuracy in TS1 (0.659) and TS3 (0.742). However, its performance in TS2 (0.589) highlighted sensitivity to environmental variability. Kappa coefficients ranged from 0.235 to 0.519, reflecting moderate reliability. While ARVI reduced Type I Errors (e.g., 0.394 in TS3), its performance was still limited by classification inaccuracies under complex conditions. MSAVI's strength lies in its reduced sensitivity to soil brightness, achieving an impressive 0.843 accuracy and 0.570 Kappa in TS1. However, its performance declined in TS3 (0.730 accuracy, 0.400 Kappa), with high Type II Errors (e.g., 0.639). Despite inconsistencies, MSAVI outperformed simpler indices like NDVI and ARVI, demonstrating its suitability for environments with sig-

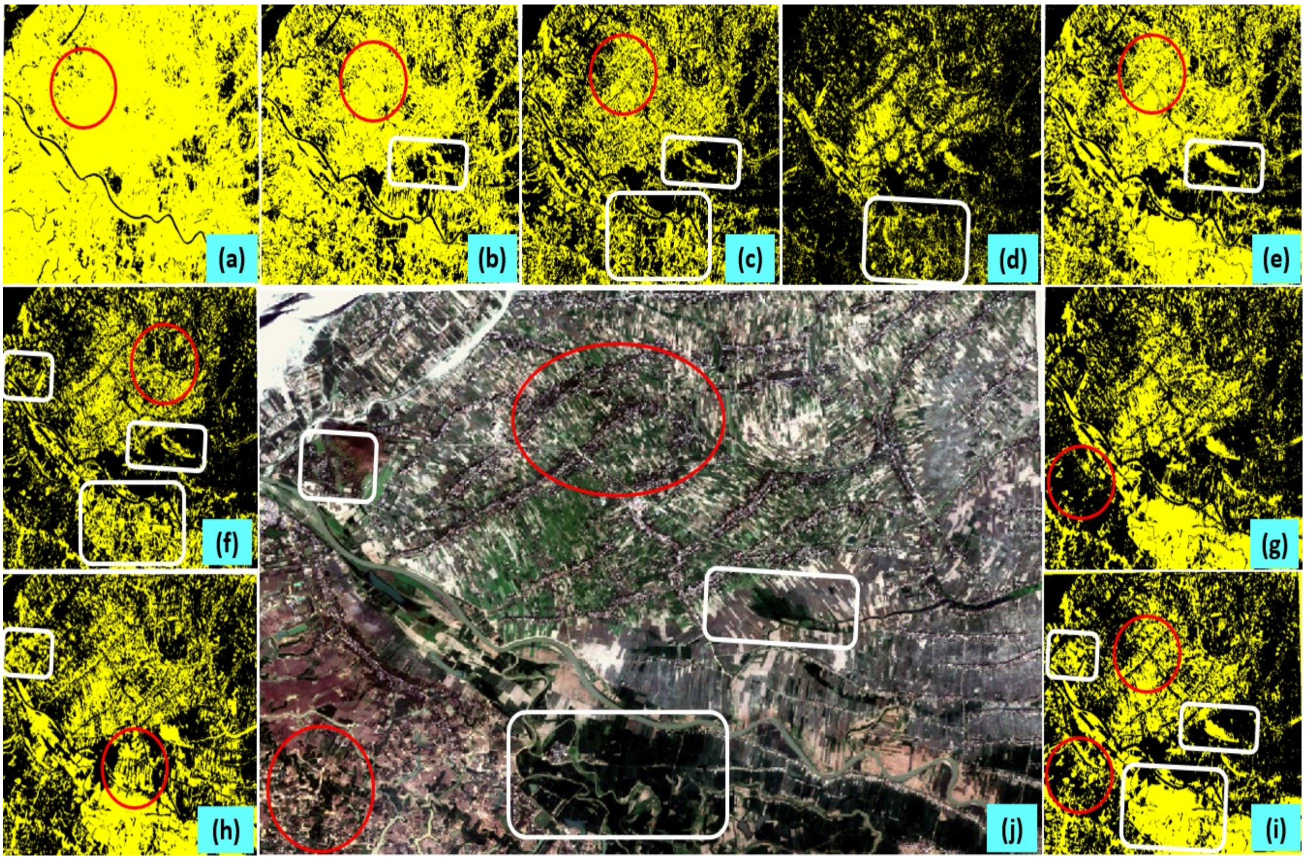

Fig. 5. *Comparison of various vegetation indices with ANVI for TS2 (a) NDVI (b) ARVI (c) MSAVI (d) IRGBVI (e) EVI (f) MGRVI (g) SAVI (h) TBDVI (i) ANVI (j) RGB Image*

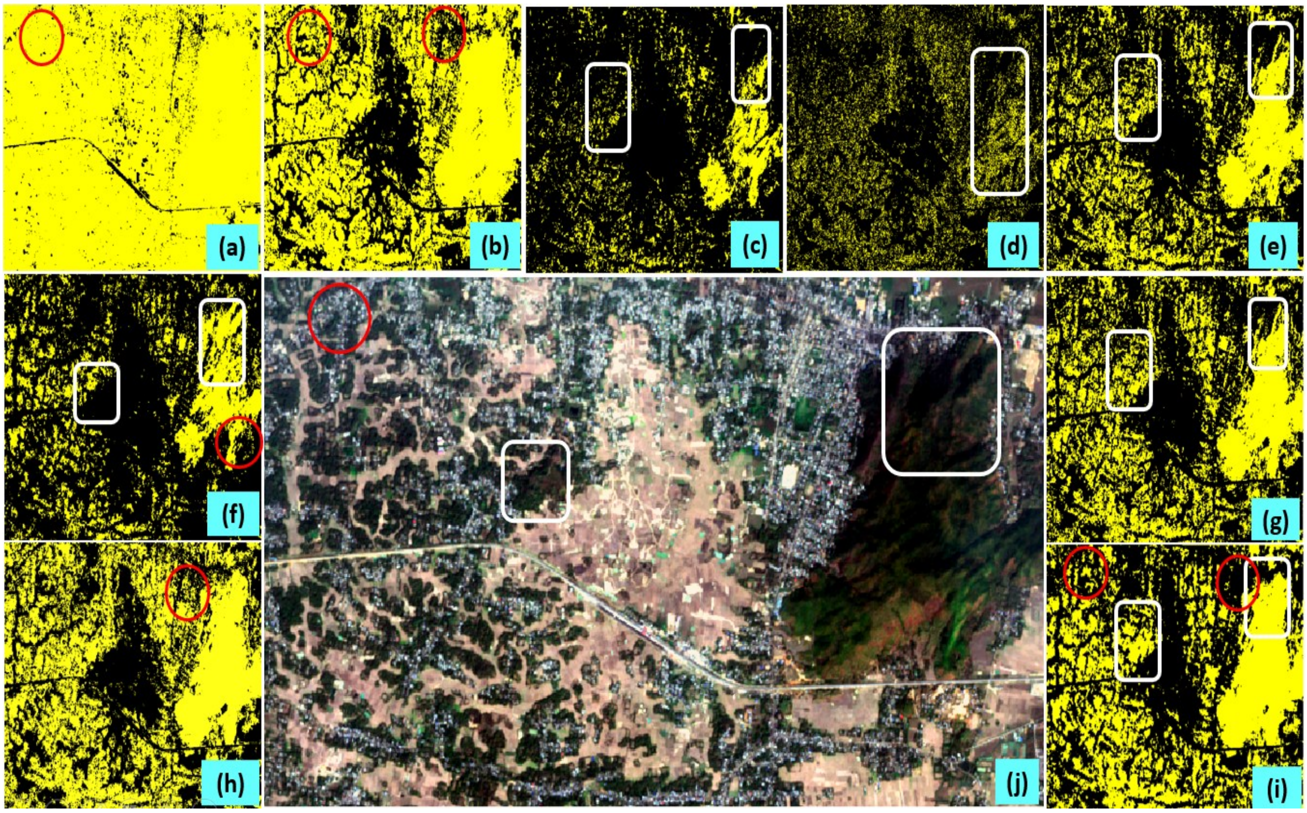

Fig 6. *Comparison of various vegetation indices with ANVI for TS3 (a) NDVI (b) MSAVI (c) ARVI (d) IRGBVI (e) SAVI (f) MGRVI (g) EVI (h) TBDVI (i) ANVI (j) RGB Image*

Table 7. Quantitative analysis of various vegetation indices with ANVI for TS1

Vegetation Indices	Overall Accuracy	Kappa Coeff.	Type I Error	Type II Error	Precision		Recall		F1-Score	
					Veg	Non Veg	Veg	Non Veg	Veg	Non Veg
NDVI	0.4409	0.1169	0.7893	0.0364	0.3496	0.9294	0.9636	0.2106	0.5130	0.3435
ARVI	0.6593	0.3726	0.4649	0.0585	0.4713	0.9540	0.9414	0.5350	0.6281	0.6856
MSAVI	0.8429	0.5695	0.0027	0.5079	0.9878	0.8168	0.4921	0.9973	0.6569	0.8981
IRGBVI	0.8591	0.6762	0.0002	0.3725	0.9952	0.8158	0.6274	0.9921	0.7710	0.8982
EVI	0.8896	0.7618	0.0662	0.1823	0.7821	0.9473	0.8875	0.8911	0.8315	0.9184
MGRVI	0.8901	0.7504	0.1089	0.1124	0.7821	0.9473	0.8875	0.8911	0.8315	0.9184
SAVI	0.8945	0.7411	0.0447	0.2436	0.8815	0.8990	0.7563	0.9552	0.8142	0.9263
TBDVI	0.9341	0.8536	0.0949	0.0032	0.8226	0.9998	0.9998	0.9051	0.9027	0.9501
ANVI	0.9686	0.9281	0.0452	0.0007	0.9068	0.9994	0.9992	0.9547	0.9511	0.9768

Table 8. Quantitative analysis of various vegetation indices with ANVI for TS2

Vegetation Indices	Overall Accuracy	Kappa Coeff.	Type I Error	Type II Error	Precision		Recall		F1-Score	
					Veg	Non Veg	Veg	Non Veg	Veg	Non Veg
NDVI	0.4231	0.0174	0.8494	0.1289	0.3496	0.9293	0.9636	0.2106	0.5130	0.3435
ARVI	0.5888	0.2348	0.5521	0.1796	0.4713	0.9540	0.9415	0.5351	0.6282	0.6856
MSAVI	0.7575	0.4916	0.2172	0.2841	0.9879	0.8169	0.4921	0.9973	0.6570	0.8981
IRGBVI	0.7590	0.5128	0.0025	0.6370	0.7617	0.9515	0.8461	0.8695	0.5206	0.6513
EVI	0.7765	0.5596	0.3028	0.0933	0.7821	0.9474	0.8876	0.8911	0.8315	0.9189
MGRVI	0.8108	0.6083	0.1935	0.1818	0.7199	0.8794	0.8181	0.8064	0.7659	0.8413
SAVI	0.8413	0.6518	0.0795	0.2889	0.8816	0.8991	0.7564	0.9553	0.8142	0.9263
TBDVI	0.8896	0.7618	0.0662	0.1829	0.8824	0.8935	0.8170	0.9337	0.8484	0.9132
ANVI	0.9706	0.9384	0.0473	0.0026	0.9068	0.9994	0.9992	0.9548	0.9511	0.9769

nificant soil interference. IRGBVI leveraged multiple spectral bands to enhance classification accuracy. It achieved 0.859 accuracy and 0.676 Kappa in TS1, and 0.833 accuracy with 0.611 Kappa in TS3. Type I Errors remained low across all sites (e.g., 0.0002 in TS1), underscoring its ability to distinguish vegetation effectively. However, moderate Type II Errors in TS3 (0.441) highlighted room for improvement under challenging conditions. SAVI demonstrated robust performance across all test sites, with accuracies of 0.895, 0.841, and 0.858 in TS1, TS2, and TS3, respectively. Its Kappa coefficients ranged from 0.652 to 0.741, reflecting high reliability. By adjusting for soil brightness, SAVI minimized classification errors, achieving a balance between sensitivity and specificity. EVI's ability to correct for atmospheric and soil background effects resulted in consistently high performance. TS1 recorded an accuracy of 0.890 and a Kappa coefficient of 0.762. Although performance dipped slightly in TS2 (0.777 accuracy, 0.560 Kappa), EVI recovered in TS3 (0.860 accuracy, 0.704 Kappa). Its robust metrics highlight its reliability across diverse conditions. MGRVI, leveraging improved greenness representation, showed promise by achieving moderate accuracy across TS1 (0.820), TS2 (0.802), and TS3 (0.812). However, its sensitivity to mixed pixel effects and subtle vegetation variations prevented it from achieving the reliability seen with indices like ANVI. TBDVI excelled in TS1, achieving the highest accuracy (0.934) and Kappa coefficient (0.854). Strong performance was also observed in TS3 (0.879 accuracy, 0.680 Kappa). Precision and Recall metrics consistently exceeded 0.99 in TS1, minimizing Type I Errors. However, sensitivity to environmental variability in TS2 (0.890 accuracy, 0.762 Kappa) indicated areas for refinement.

The proposed ANVI consistently outperformed all other indices, achieving the highest overall accuracy and Kappa coefficients across all test sites. In TS1, ANVI recorded 0.969 accuracy and 0.928 Kappa, with similar results in TS2 (0.971 accuracy, 0.938 Kappa) and TS3 (0.963 accuracy, 0.932 Kappa). Precision (0.999) and Recall (0.998) metrics highlight its unmatched classification performance. By minimizing Type I and II Errors (e.g., 0.045 and 0.0007 in TS1), ANVI demonstrated exceptional reliability, adaptability, and robustness under diverse environmental conditions.Notably, the parameter λ was empirically set to 2, as it provided the most stable and optimal classification results across all

Table 9. Quantitative analysis of various vegetation indices with ANVI for TS3

Vegetation Indices	Overall Accuracy	Kappa Coeff.	Type I Error	Type II Error	Precision		Recall		F1-Score	
					Veg	Non Veg	Veg	Non Veg	Veg	Non Veg
NDVI	0.4302	0.0577	0.9190	0.0072	0.4014	0.9477	0.9928	0.0810	0.5717	0.1492
MSAVI	0.7301	0.4001	0.0079	0.6395	0.9658	0.7142	0.3605	0.9921	0.5250	0.8305
ARVI	0.7420	0.5197	0.3948	0.0377	0.6021	0.9628	0.9623	0.6052	0.7407	0.7432
IRGBVI	0.8328	0.6109	0.0582	0.4419	0.8451	0.7881	0.5580	0.9988	0.7163	0.8815
SAVI	0.8578	0.6910	0.0726	0.2545	0.8645	0.8544	0.7455	0.9274	0.8006	0.8894
MGRVI	0.8582	0.6870	0.2099	0.0005	0.6771	0.9998	0.9991	0.7900	0.8074	0.8827
EVI	0.8597	0.7035	0.1150	0.1810	0.8156	0.8873	0.8190	0.8850	0.8173	0.8862
TBDVI	0.8792	0.6801	0.0020	0.3950	0.9925	0.8518	0.6049	0.9898	0.7538	0.9199
ANVI	0.9628	0.9323	0.0427	0.0201	0.9001	0.9990	0.9980	0.9073	0.9305	0.9514

test sites. Its sophisticated integration of spectral bands addresses atmospheric and soil brightness challenges effectively. The comparative analysis highlights ANVI's dominance over traditional indices, consistently delivering the highest accuracy, Kappa coefficients, and F1-Scores across all test sites. ANVI stands out as the most reliable and adaptable vegetation index for land cover classification, outperforming several traditional indices. While other indices showed moderate to strong performance under specific conditions, their limitations in handling atmospheric effects, soil brightness, or environmental variability were evident. ANVI's integration of diverse spectral bands ensures unmatched accuracy, robustness, and adaptability, making it a superior choice for remote sensing applications.

Conclusion

The proposed vegetation index introduced in this research marked a significant advancement in vegetation mapping, addressing key limitations observed in existing methods, especially in complex landscapes with spectral overlaps and varying environmental conditions. By effectively utilizing the spectral richness of multispectral bands, the new index demonstrated improved accuracy and reliability in vegetation extraction, particularly in challenging areas where traditional indices show reduced performance. The index was designed for robustness across diverse terrains, ensuring consistent vegetation mapping, even in regions with intricate spatial patterns. Its application extends to precision agriculture, offering refined insights into vegetation health, moisture levels, and nutrient status, thereby supporting better-informed agricultural practices. Overall, the proposed index offers a valuable contribution to remote sensing and vegetation monitoring, facilitating more precise environmental management and aiding in sustainable development efforts.

ACKNOWLEDGEMENTS

We sincerely thank the current director, Dr. S. P. Aggarwal, and former director, Shri P L N Raju, of NESAC for their support and encouragement. Our gratitude also extends to Girijananda Chowdhury Institute of Management and Technology (now Girijananda Chowdhury University) and Assam Science and Technology University for providing the platform for this research. We appreciate the valuable suggestions and comments from the reviewers and editors.

Conflicts of Interest

The authors declared that they have no conflict of interest

Funding

The authors had no relevant financial or non-financial interests to disclose.

REFERENCES

1. Alkama, R., Forzieri, G. & Duveiller, G. (2022**).** Vegetation -based climate mitigation in a warmer and greener World. *NatCommun*13, 606.https://doi.org/10.1038/s41467-022-28305-9
2. Anderson, K.; Hancock, S.; Disney, M. & Gaston, K.J. (2015) Is waveform worth it? A comparison of LiDAR approaches for vegetation and landscape characterization*.* *Remote Sens. Ecol. Conserv*. 2, 5–15. https://doi.org/10.1002/rse2.8
3. Ain, A., Gogoi, M. & Chutia, D. (2021). CNN-enhanced multi-indices patch-based classification: A case study of Guwahati city. *International Journal of Scientific and Research Publications* (IJSRP), 9, 1824–1840. https://doi.org/10.22214/ijraset.2021.39593
4. Ain, A., Gogoi, M. & Chutia, D. Multispectral Satellite Data Classification Using Rank Correlation Similarity Index and Automatic Labeling Technique. (2024) *Sn Comput. Sci.* 5,

1073. https://doi.org/10.1007/s42979-024-03380-5

5. Au, K. N. (2023). NDVI assessment versus two impact factors analysis (separate analysis based on chlorophyll content and leaf cellular structure): which method is more effective to detect declining health of an individual tree? *Geocarto International,* 38(1). https://doi.org/10.1080/10106049.2023.2229773
6. Bendig, J., Yu, K., Aasen, H., Bolten, A., Bennertz, S., Broscheit, J., Gnyp, M. & Bareth, G. (2015). Combining UAV-based plant height from crop surface models, visible, and near-infrared vegetation indices for biomass monitoring in barley. *International Journal of Applied Earth Observation and Geoinformation,* 39, 79–87. https://doi.org/10.1016/j.jag.2015.02.012
7. Buma, W., Abelev, A., & Merrick, T. (2024). Vegetation spectra as an integrated measure to explain underlying soil characteristics: A review of recent advances. *Frontiers in Environmental Science,* 12. https://doi.org/10.3389/fenvs.2024.1430818
8. Ceccato, P., Flasse, S., Tarantola, S., Jacquemoud, S. & Grégoire, J.-M. (2001). Detecting vegetation leaf water content using reflectance in the optical domain. *Remote Sensing of Environment,* 77, 22–33. https://doi.org/10.1016/S0034-4257(01)00191-2
9. Chen, C., Yuan, X., Gan, S., Luo, W., Bi, R., Li, R., & Gao, S. (2024). A new vegetation index based on UAV for extracting plateau vegetation information. *International Journal of Applied Earth Observation and Geoinformation*, 128, 103668. https://doi.org/10.1016/j.jag.2024.103668
10. Clevers, J. & Gitelson, A. (2013). Remote estimation of crop and grass chlorophyll and nitrogen content using red-edge bands on Sentinel-2 and -3. *International Journal of Applied Earth Observation and Geoinformation*, 23, 344–351. https://doi.org/10.1016/j.jag.2012.10.008
11. Congedo, L., (2021). Semi-Automatic Classification Plugin: A Python tool for the download and processing of remote sensing images in QGIS. *Journal of Open Source Software*, 6(64), 3172, https://doi.org/10.21105/joss.03172
12. Delegido, J., Verrelst, J., Meza, C., Rivera, J., Alonso, L. & Moreno, J. (2013). A red-edge spectral index for remote sensing estimation of green LAI over agroecosystems. *European Journal of Agronomy*, 46, 42–52. https://doi.org/10.1016/j.eja.2012.12.001
13. EOS EVI (2024). Enhanced Vegetation Index (EVI). Retrieved 21 Dec 2024, from https://eos.com/blog/vegetation-indices/
14. EOS MSAVI (2024). Modified Soil-Adjusted Vegetation Index (MSAVI). Retrieved 21 Dec 2024, from https://eos.com/make-an-analysis/msavi/
15. Feyisa, G., Meilby, H., Fensholt, R. & Proud, S. (2014). Automated Water Extraction Index: A new technique for surface water mapping using Landsat imagery. *Remote Sensing of Environment*, 140, 23–35. https://doi.org/10.1016/j.rse.2013.08.029
16. Fu, Z., Jiang, J., Gao, Y., Krienke, B., Wang, M., Zhong, K., Cao, Q., Tian, Y., Zhu, Y., Cao, W. & Liu, X. (2020). Wheat growth monitoring and yield estimation based on multi-rotor unmanned aerial vehicle. *Remote Sensing*, 12, 508. https://doi.org/10.3390/rs12030508
17. Gao, B.-C. (1996). NDWI—a normalized difference water index for remote sensing of vegetation liquid water from space. Remote Sensing of Environment, 58(3), 257–266. https://doi.org/10.1016/S0034-4257(96)00067-3
18. Gessesse, A.A. & Melesse, A.M. (2019). Temporal relationships between time series CHIRPS-rainfall estimation and eMODIS-NDVI satellite images in Amhara Region, Ethiopia. Elsevier, pp. 81–92. DOI:10.1016/B978-0-12-815998-9.00008-7
19. Gitelson, A.A., Kaufman, Y.J. & Merzlyak, M.N. (1996). Use of a green channel in remote sensing of global vegetation from EOS-MODIS. *Remote Sensing of Environment*, 58(3), 289–298. https://doi.org/10.1016/S0034-4257(96)00072-7
20. Hmimina, G., Dufrêne, E., Pontailler, J.-Y., Delpierre, N., Aubinet, M., Caquet, B., de Grandcourt, A., Burban, B., Flechard, C., Granier, A., Gross, P., Heinesch, B., Longdoz, B., Moureaux, C., Ourcival, J.-M., Rambal, S., Saint André, L. & Soudani, K. (2013). Evaluation of the potential of MODIS satellite data to predict vegetation phenology in different biomes: An investigation using ground-based NDVI measurements. *Remote Sensing of Environment*, 132, 145–158. https://doi.org/10.1016/j.rse.2013.01.010
21. Huete, A.R. (1988). A soil-adjusted vegetation index (SAVI). *Remote Sensing of Environment*, 25(3), 295–309. https://doi.org/10.1016/0034-4257(88)90106-X
22. Huete, A., Didan, K., Miura, T., Rodriguez, E.P., Gao, X. & Ferreira, L.G. (2002). Overview of the radiometric and biophysical performance of the MODIS vegetation indices. *Remote Sensing of Environment,* 83(1-2), 195–213. https://doi.org/10.1016/S0034-4257(02)00096-2
23. Jiang, Z., Huete, A.R., Didan, K. & Miura, T. (2008). Development of a two-band enhanced vegetation index without a blue band. Remote Sensing of Environment, 112 (10), 3833–3845. https://doi.org/10.1016/j.rse.2008.06.006
24. Kaufman, Y.J. & Tanre, D. (1992). Atmospherically resistant vegetation index (ARVI) for EOS-MODIS. *IEEE Transactions on Geoscience and Remote Sensing*, 30(2), 261–270. doi: 10.1109/36.134076
25. Key, Carl & Benson, Nate. (2006). Landscape Assessment: Ground measure of severity, the Composite Burn Index; and Remote sensing of severity, the Normalized Burn Ratio. Retrieved 21 Dec 2024 from https://pubs.usgs.gov/publication/2002085
26. Khalid, H.W., Khalil, R.M.Z. & Qureshi, M.A. (2021). Evaluating spectral indices for water bodies extraction in Western Tibetan Plateau. *The Egyptian Journal of Remote Sensing and Space Science,* 24(3), 619–634. https://doi.org/10.1016/j.ejrs.2021.09.003
27. Lane, C., Liu, H., Autrey, B., Anenkhonov, O., Chepinoga, V. & Wu, Q. (2014). Improved wetland classification using eight-b& high resolution satellite imagery and a hybrid approach. *Remote Sensing*, 6, 12187–12216. https://doi.org/10.3390/rs61212187
28. Llobera, M. (2007). Modeling visibility through vegetation. *International Journal of Geographical Information Science*, 21(7), 799–810. https://doi.org/10.1080/13658810601169865
29. Li, J., Peng, S. & Li, Z. (2017). Detecting and attributing vegetation changes on China's Loess Plateau. *Agricultural and Forest Meteorology*, 247, 260–270. doi: https://doi.org/10.1016/j.agrformet.2017.08.005
30. Li, W., Clark, B., Taylor, J., Kendall, H., Jones, G., Li, Z., Jin, S., Zhao, C., Yang, G., Shuai, C., et al. (2020). A hybrid modelling approach to understanding adoption of

precision agriculture technologies in Chinese cropping systems. *Computers and Electronics in Agriculture*, 172, 105305. https://doi.org/10.1016/j.compag.2020.105305

31. Lu, D., Li, G., Kuang, W., & Moran, E. (2013). Methods to extract impervious surface areas from satellite images. *International Journal of Digital Earth*, 7(2), 93–112. https://doi.org/10.1080/17538947.2013.866173
32. McFeeters, S.K. (1996) The Use of the Normalized Difference Water Index (NDWI) in the Delineation of Open Water Features. *International Journal of Remote Sensing*, 17, 1425-1432. http://dx.doi.org/10.1080/01431169608948714
33. Makarieva, Anastassia & Gorshkov, Victor. (2010). The Biotic Pump: Condensation, atmospheric dynamics and climate. International Journal of Water. 5. 365-385. 10.1504/IJW.2010.038729
34. Markham, B.L. & Barker, J.L. (1986). Landsat MSS and TM post-calibration dynamic ranges, exoatmospheric reflectance, and at-satellite temperatures. *Landsat Technical Notes*, Vol. I, August. Retrieved 21 Dec 2024 from https://typeset.io/papers/landsat-mss-and-tm-post-calibration-dynamic-ranges-31sa8wdivs on 21 Dec 2024
35. Mashala, M., Dube, T., Mudereri, B., Ayisi, K. & Ramudzuli, M. (2023). A systematic review on advancements in remote sensing for assessing and monitoring land use and land cover changes impacts on surface water resources in semi-arid tropical environments. *Remote Sensing*, 15(16), 3926. https://doi.org/10.3390/rs15163926
36. Mondejar, J.P. & Tongco, A.F. (2019). Near infrared band of Landsat 8 as water index: A case study around Cordova and Lapu-Lapu City, Cebu. *Sustain Environ Res.,* 29, 16. https://doi.org/10.1186/s42834-019-0016-5
37. Papoutsis, K., Mathioudakis, M.M., Hasperué, J.H. & Ziogas, V. (2019) Non-Chemical Treatments for Preventing the Postharvest Fungal Rotting of Citrus Caused by Penicillium digitatum (Green Mold) and Penicillium italicum (Blue Mold). *Trends in Food Science & Technology*, 86, 479-491. https://doi.org/10.1016/j.tifs.2019.02.053
38. Poursanidis, D., Chrysoulakis, N., & Mitraka, Z., (2015). Landsat 8 vs. Landsat 5: A comparison based on urban and peri-urban land cover mapping. *International Journal of Applied Earth Observation and Geoinformation,* 35, 259–269. https://doi.org/10.1016/j.jag.2014.09.010
39. Qi, J., Chehbouni, A., Huete, A., Kerr, Y., & Sorooshian, S., (1994). A modified soil adjusted vegetation index. Remote Sensing of Environment, 48(2), 119–126.https://doi.org/10.1016/0034-4257(94)90134-1
40. Rokni, K., Ahmad, A., Selamat, A. & Hazini, S., (2014). Water feature extraction and change detection using multitemporal Landsat imagery. *Remote Sensing*, 6, pp.4173–4189. https://doi.org/10.3390/rs6054173
41. Roujean, J.-L., & Breon, F.-M., (1995). Estimating PAR absorbed by vegetation from bidirectional reflectance measurements. *Remote Sensing of Environment*, 51(3), 375–384. https://doi.org/10.1016/0034-4257(94)00114-3
42. Rouse, J.W., Haas, R.H., Schell, J.A. & Deering, D.W. (1974). Monitoring vegetation systems in the great plains with ERTS. *Proceedings of the Third Earth Resources Technology Satellite (ERTS) Symposium,* 1, 309–317. Retrieved 21 Dec 2024 from https://api.semanticscholar.org/CorpusID:133358670
43. Roy, P., (1989). Spectral reflectance characteristics of vegetation and their use in estimating productive potential. *Proceedings of the Indian Academy of Sciences (Plant Sciences),* 99, 59–81. https://doi.org/10.1007/BF03053419
44. Sentinel Hub, (2024). Atmospherically Resistant Vegetation Index (ARVI). Retrieved 21 Dec 2024, from https://custom-scripts.sentinel-hub.com/custom-scripts/sentinel-2/arvi
45. Shen, M., Tang, Y., Klein, J., Zhang, P., Gu, S., Shimono, A., & Chen, J., (2008). Estimation of aboveground biomass using in situ hyperspectral measurements in five major grassland ecosystems on the Tibetan Plateau. Journal of Plant Ecology, 1. https://doi.org/10.1093/jpe/rtn025
46. Singh, M.R., & Bhide, A., (2016). A review of image retrieval using different types of interpolation techniques. *International Research Journal of Engineering and Technology (IRJET),* 3(12). Retrieved 21 Dec 2024, from: https://www.irjet.net/archives/V3/i12/IRJET-V3I12313.pdf
47. Sun, G., Jiao, Z., Zhang, A., Li, F., Fu, H., & Li, Z., (2021). Hyperspectral image-based vegetation index (HSVI): A new vegetation index for urban ecological research. International Journal of Applied Earth Observation and Geoinformation, 103, 102529. https://doi.org/10.1016/j.jag.2021.102529
48. Tempa, K., & Aryal, K., (2022). Semi-automatic classification for rapid delineation of the geohazard-prone areas using Sentinel-2 satellite imagery. *SN Applied Sciences*, 4, 141. https://doi.org/10.1007/s42452-022-05028-6
49. Tucker, C.J. (1979). Red and photographic infrared linear combinations for monitoring vegetation. Remote Sensing of Environment, 8(2), 127–150. http://dx.doi.org/10.1016/0034-4257(79)90013-0
50. USGS NDVI,(2024). *Normalized Difference Vegetation Index (NDVI).* Retrieved July 15, 2024, from https://www.usgs.gov/special-topics/remote-sensing-phenology/science/ndvi-foundation-remote-sensing-phenology.
51. USGS SAVI,(2024). Soil Adjusted Vegetation Index (SAVI). Retrieved July 15, 2024, from https://www.usgs.gov/landsat-missions/landsat-soil-adjusted-vegetation-index.
52. Ustuner, M., & Sanli, F., (2015). Testing the sensitivity of vegetation indices for crop type classification using RapidEye imagery. In: FIG Working Week 2015, Sofia, Bulgaria, May 17-21. Retrieved 21 Dec 2024 from https://www.fig.net/resources/proceedings/fig_proceedings/fig2015/papers/ts02e/TS02E_ustuner_balik_sanli_7701.pdf
53. Wang, X., Xu, H., Zhou, J., Fang, X., Shuai, S., & Yang, X., (2024). Analysis of vegetation canopy spectral features and species discrimination in reclamation mining area using in situ hyperspectral data. *Remote Sensing*, 16, 2372. https://doi.org/10.3390/rs16132372
54. Wang, J., Zhao, W., Wang, G., & Pereira, P., (2022). Afforestation changes the trade-off between soil moisture and plant species diversity in different vegetation zones on the Loess Plateau. *CATENA,* 219, 106583. 10.1016/j.catena.2022.106583
55. Weng, Q., (2012). Remote sensing of impervious surface in the urban areas: Requirements, methods, and trends. *Remote Sensing of Environment*, 117, 34–49. https://doi.org/10.1016/j.rse.2011.02.030

56. Wilson, E.H. & Sader, S.A., (2002). Detection of forest harvest type using multiple dates of Landsat TM imagery. *Remote Sensing of Environment*, 80, pp.385–396. http://dx.doi.org/10.1016/S0034-4257(01)00318-2
57. Xie, Y., Sha, Z., & Yu, M.,(2008) Remote sensing imagery in vegetation mapping: A review, *Journal of Plant Ecology,* 1 (1), March Pages 9–23, https://doi.org/10.1093/jpe/rtm005
58. Xu, H., (2006). Modification of normalised difference water index (NDWI) to enhance open water features in remotely sensed imagery. *International Journal of Remote Sensing*, 27(14), pp.3025–3033. https://doi.org/10.1080/01431160600589179
59. Xue, J. & Su, B., (2017). Significant remote sensing vegetation indices: A review of developments and applications. *Journal of Sensors*, 1–17. https://doi.org/10.1155/2017/1353691
60. Yan, D., Huang, C., Ma, N., & Zhang, Y., (2020). Improved Landsat-based water and snow indices for extracting lake and snow cover/glacier in the Tibetan Plateau. *Water,* 12(5), 1339. https://doi.org/10.3390/w12051339
61. Yaseen, M., Fan, G., Zhou, X., Long, W., & Feng, G., (2022). Plant diversity and soil nutrients in a tropical coastal secondary forest: Association, ordination, and sampling year differences. *Forests,* 13, 376 https://doi.org/10.3390/f13030376
62. Zagajewski, B., Tommervik, H., Bjerke, J., Raczko, E., Bochenek, Z., Kios, A., Jarocinska, A., Lavender, S., & Ziolkowski, D., (2017). Intraspecific differences in spectral reflectance curves as indicators of reduced vitality in high-arctic plants. *Remote Sensing*, 9, 1289. https://doi.org/10.3390/rs9121289
63. Zhai, K., Wu, X., Qin, Y. & Du, P., (2015). Comparison of surface water extraction performances of different classic water indices using OLI and TM imageries in different situations. *Geo-spatial Information Science*, 18(3). https://doi.org/10.1080/10095020.2015.1017911
64. Zhao, C., Pan, Y., Ren, S., Gao, Y., Wu, H., & Ma, G. (2024). Accurate vegetation destruction detection using remote sensing imagery based on the three-band difference vegetation index (TBDVI) and dual-temporal detection method. *International Journal of Applied Earth Observation and Geoinformation*, 127, 103669. https://doi.org/10.1016/j.jag.2024.103669